Inorganic Chemistry

ARTICLE

pubs.acs.org/IC

Excited-State Properties of Heteroleptic Iridium(III) Complexes Bearing Aromatic Hydrocarbons with Extended Cores

Fabian Spaenig,[†] Jean-Hubert Olivier,[‡] Valentina Prusakova,[†] Pascal Retailleau,[§] Raymond Ziessel,*[,‡] and Felix N. Castellano*[,†]

[†]Department of Chemistry and Center for Photochemical Sciences, Bowling Green State University, Bowling Green, Ohio 43403, United States

[‡]Laboratoire de Chimie Organique et Spectroscopies Avancées (LCOSA), associé au Centre National de la Recherche Scientifique (UMR 7515-CNRS), Ecole de Chimie, Polymères, Matériaux (ECPM), 25 rue Becquerel, 67087 Strasbourg Cedex 02, France

[§]Laboratoire de Crystallochimie, ICSN-CNRS, Bât 27, 1 avenue de la Terrasse, 91198 Gif-sur-Yvette Cedex, France

S *Supporting Information*

ABSTRACT: The synthesis, complete structural characterization, electrochemistry, and excited-state dynamics of a series of four bis-heteroleptic iridium(III) charge-transfer complexes composed of a single acac-functionalized and two ortho-metalated 2-phenylpyridine ligands. The formed iodophenyl complex (**2**) was used as a metallosynthon to introduce extended-core ethynyltolyl (**3**), ethynylpyrene (**4**), and ethynylperylene (**5**) residues into these structures projecting from the acac ancillary ligand. Static and dynamic photoluminescence along with ultrafast and conventional transient absorption measurements in conjunction with cyclic voltammetry were employed to elucidate the nature of the intramolecular energy-transfer processes occurring in the excited states of polychromophores **4** and **5** and are directly compared with those of model complexes **2** and **3**. Upon charge-transfer excitation of these molecules, the long-lived triplet-state metal-to-ligand charge-transfer (^{3}MLCT)-based photoluminescence readily observed in **2** and **3** ($\tau = 1\ \mu$s) is nearly quantitatively quenched, resulting from production of the associated triplet intraligand (^{3}IL) excited states in **4** and **5** through intramolecular triplet−triplet energy transfer. The respective formation of the extended-core ^{3*}pyrenyl and ^{3*}perylenyl-localized excited states in **4** and **5** is confirmed by their ultrafast excited-state evolution, which ultimately generates features associated with these ^{3}IL excited states and their greatly extended excited-state lifetimes with respect to the parent complexes **2** and **3**.

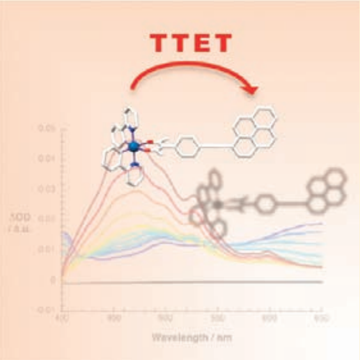

INTRODUCTION

Third-row transition-metal charge-transfer complexes, particularly those containing platinum(II) or iridium(III), have recently attracted considerable attention because they can facilitate efficient intersystem crossing, ultimately leading to the efficient population of the molecule's triplet excited state.[1−5] Here the spin-forbidden nature of the radiative relaxation process is also relaxed, resulting in a high phosphorescence quantum efficiency from the lowest triplet excited state. Minor structural variation within certain platinum complexes often alters the resultant photophysical properties,[1,4] and judicious tuning of the surrounding ligands has even enabled near-IR phosphorescence emission to be observed, potentially an attractive alternative to more conventional organic fluorophores.[6,7] Similarly, grafting ancillary polyaromatic modules to the resultant platinum(II) complex enables efficient intramolecular energy transfer to the low-lying triplet of the organic fragment, producing its corresponding photophysics.[8−14] On the other hand, iridium(III) complexes enable broader tuning possibilities because of their increased ligand-field stabilization energy and pronounced decoupling with metal-centered excited states, which are essentially thermally inaccessible.[15,16] For instance, homoleptic iridium(III) complexes such as $Ir(ppy)_3$ possess desirable spectroscopic properties such as long-lived emitting states and quantitative photoluminescence quantum efficiencies.[15] Homoleptic and heteroleptic iridium(III) complexes have also been used extensively for sensing and bioimaging,[17−19] as the light-emitting component in organic light-emitting devices,[20−23] achieving nearly 100% internal quantum efficiency,[24] and in upconversion schemes.[25] Furthermore, the kinetic inertness of the coordination sphere permits the construction of asymmetric molecules[26] but also the use of dedicated complexes as metallosynthons to graft additional functional modules such as organic chromophores, using the concept of "chemistry on the complex".[27−30]

Cyclometalated iridium(III) complexes are robust, easy to produce, synthetically versatile, and photochemically and thermally stable and display desirable photophysical properties.[31−33] These attractive features prompted us to combine an orthometalated iridium(III) precursor with (phenyliodo)acetylacetonate

Received: June 29, 2011
Published: September 02, 2011

recently prepared using copper-promoted cross-coupling reactions.[34] We speculated that selected functionalization of the iodo function with alkyne chemistry would provide a range of opportunities to tether photoactive polyaromatic residues in such a way that intramolecular energy transfer from the charge-transfer complex to the appended energy acceptor would be efficient. Fortunately, unsubstituted acetylacetonate (acac)-based iridium(III) complexes do exist, and the majority of [(ppy)$_2$Ir(acac)] complexes indeed phosphoresce with high quantum yields and exhibit microsecond lifetimes.[35] Furthermore, when the appropriate ancillary ligand was chosen, green-to-red emission characteristics could potentially be synthetically tailored into the structure.[21,22,36]

Herein, we describe the synthesis and complete structural and photophysical characterization of a series of *bis*-heteroleptic Ir(III) chromophores linked to ethynyltolyl (**3**), ethynylpyrene (**4**), and ethynylperylene (**5**), each projecting from an appended acac ligand. The former serves as a control molecule where the possibility of low-lying organic fragment-based triplet state photophysics is deleted and the two latter molecules were purposely designed so that the corresponding hydrocarbon triplet states would become populated. Indeed, this is the case and regardless of the excitation wavelength utilized, the extended-core aromatic hydrocarbon-based ligand-localized triplet excited state is exclusively produced in **4** and **5**, clearly demonstrated by ultrafast and conventional transient absorption spectroscopy. Although the resultant ligand-localized excited states in **4** and **5** are long-lived, these triplet states are unfortunately dark and do not phosphoresce at room temperature (RT).

■ EXPERIMENTAL SECTION

General Procedures. All reactions were performed under a dry atmosphere of argon using standard Schlenk techniques. All chemicals were used as received from commercial sources without further purification unless otherwise stated. CH_2Cl_2 and CH_3CN were distilled from P_2O_5 under an argon atmosphere. Tetrahydrofuran (THF) was distilled from sodium benzophenone under an argon atmosphere. ^{1}H NMR (300.1 MHz) and ^{13}C NMR (75.5 MHz) spectra were recorded at RT on a Bruker Avance 300 MHz spectrometer; ^{1}H NMR (200.1 MHz) and ^{13}C NMR (50.5 MHz) spectra were recorded at RT on a Bruker Avance 200 MHz spectrometer, using perdeuteriated solvents as internal standards. Fourier transform infrared spectra were recorded on a ATR plate. Fast atom bombardement (FAB, positive mode) mass spectra were recorded with a ZAB-HF-VB analytical apparatus with *m*-nitrobenzyl alcohol as the matrix. Chromatographic separations/purifications were performed using 40−63 μm silica gel. Thin-layer chromatography was performed on silica gel plates coated with a fluorescent indicator.

X-ray Structure Determination. X-ray crystallographic data were recorded at RT on a Nonius-Bruker Kappa CCD diffractometer using graphite-monochromated Mo Kα radiation (λ = 0.7107 Å). Complete data sets were measured according to a *j* and *w* scan strategy derived by the *COLLECT*[37] suite once the cell parameters were estimated using *DENZO*[38] from a preliminary 10° *j* scan. In the case of **4**, this air-unstable crystal was mounted into a sealed capillary that restricted a full rotation scan around the spindle axis, resulting in quick and incomplete data collection. Data were then integrated by *DENZO*[38] and corrected for Lorentz and polarization effects. An empirical absorption correction based on a comparison of the redundant and equivalent reflections was applied using *SCALEPACK*.[38] Both structures (**2** and **4**) could be solved by direct methods[1,4] and were expanded using Fourier techniques.[39] All non-hydrogen atoms were refined anisotropically, while the hydrogen atoms were principally located on difference Fourier syntheses but refined isotropically with a riding model and with $U_{iso}(H) = 1.2U_{eq}(C)$ (or 1.5 for the methyl group). The *SQUEEZE* option from *PLATON*[40] was used to treat the presence of disordered solvent molecules in **4**. Their contribution to the diffraction pattern supposedly consisted of two molecules of the Et_2O solvent, removed and modified by $F_o{}^2$ written to a new *HKL* file.

For complex **2** ($C_{33}H_{26}IIrN_2O_2 \cdot 2C_2H_3N$): space group, triclinic $P\bar{1}$; a = 10.124(4) Å, b = 13.335(5) Å, c = 13.893(5) Å, α = 110.81(2)°, β = 100.08(2)°, γ = 93.96(1)°, V = 1708.5(11) Å^3, Z = 2, F(000) = 856, D_{calc} = 1.718 g cm^{-3}, μ = 4.848 mm^{-1}, independent reflections 6972 (R_{int} = 0.038), observed reflections 5475 [$I > 2\sigma(I)$], refinement method; full-matrix least squares on F^2, data/restraints/parameters, 6972/3/410, R1 = 0.0359, R_w = 0.0747, GOF on F^2 = 1.028, Δr_{min} and r_{max} are +0.762 and −0.897 e A^{-3}.

For complex **4** ($C_5H_{35}IrN_2O_2 \cdot 2C_4H_{10}O$): M_r = 1048.25; space group, triclinic, $P\bar{1}$; a = 9.516(4) Å, b = 11.742(6) Å, c = 20.778(12) Å, α = 105.31(5)°, β = 90.39(4)°, γ = 91.63(4)°, V = 2238(2) Å^3, Z = 2, F(000) = 1064, D_{calc} = 1.555 g cm^{-3}, μ = 3.037 mm^{-1}, independent reflections 7964 (R_{int} = 0.0326), observed reflections 6281 [$I > 2\sigma(I)$], refinement method; full-matrix least squares on F^2, data/restraints/parameters, 7964/160/507, R1 = 0.0482, R_w = 0.1111, GOF on F^2 = 1.043, Δr_{min} and r_{max} are +0.901 and −1.474 e A^{-3}. Supplementary data in the form of CIFs have been deposited with the Cambridge Crystallographic Data Centre [CCDC 800954 (complex **2**) and 800955 (complex **4**)]. Copies of the data can be obtained, free of charge, upon application to CCDC, 12 Union Road, Cambridge CB2 IEZ, U.K. [fax +44(0)-1223-336033 or e-mail deposit@ccdc.cam.ac.uk].

Reagents. *t*-BuOK, copper iodide, benzene, 2-phenylpyridine (ppy), and triethylamine were purchased from commercial sources and used without further purification. Dichloromethane was dried over P_2O_5 and distilled under an argon atmosphere immediately prior to use. 3-(4-Iodobenzyl)-2,4-pentanedione,[34] [(ppy)$_2$IrCl]$_2$,[41] [Pd(PPh$_3$)$_2$Cl$_2$],[42] 1-ethynylpyrene,[43] and 3-ethynylperylene[44] were prepared and purified according to literature procedures.

General Procedure for the Sonogashira Cross-Coupling Reaction. A Schlenk flask was charged with [(ppy)$_2$Ir(acacPhI)] (**2**), the appropriate ethynyl derivative, benzene, and triethylamine. The mixture was argon-degassed for 30 min, then CuI and [Pd(PPh$_3$)$_2$Cl$_2$] were introduced, and the reaction mixture was stirred at RT for 18 h. The solvents were evaporated, and the residue was treated with water and extracted with dichloromethane. The organic extracts were washed with water, followed by saturated brine, and finally dried over Na_2SO_4. After rotary evaporation, the residue was purified by column chromatography.

*Complex [(ppy)$_2$Ir(acacPhI)] (**2**).* A solution of 3-(4-iodobenzyl)-2,4-pentanedione (500 mg, 1.650 mmol) in 50 mL of anhydrous dichloromethane was cooled to 0 °C, and *t*-BuOK (192 mg, 1.700 mmol) was added in one portion. The reaction mixture was stirred for 2 h before **1** (884 mg, 0.825 mmol) was added, and the resulting reaction mixture was allowed to warm up to RT and stirred an additional 2 h. The resultant solution was poured on 50 mL of a saturated NH_4Cl solution and extracted with CH_2Cl_2 (3 × 40 mL). The organic phase was washed with water and brine and finally dried over sodium sulfate. The solvents were removed under vacuum. Purification by chromatography on aluminum oxide (40:60 ethyle acetate/petroleum ether) afforded **2** as a yellow solid (1.136 g, 86%). ^{1}H NMR (400 MHz, CD_2Cl_2): δ 8.62 (dd, 2H, ^3J = 6.4 Hz, ^4J = 0.8 Hz), 7.92 (d, 2H, ^3J = 8.4 Hz), 7.83 (dt, 2H, ^3J = 7.2 Hz, ^4J = 1.6 Hz), 7.60 (dd, 2H, ^3J = 6.4 Hz, ^4J = 1.6 Hz), 7.29 (AB quartet, 4H, ^{AB}J = 8.4 Hz, $\nu\,\delta_{AB}$ = 304.3 Hz), 7.26 (dt, 2H, ^3J = 6.4 Hz, ^4J = 1.2 Hz), 6.85 (dt, 2H, ^3J = 7.6 Hz, ^4J = 1.2 Hz), 6.69 (dt, 2H, ^3J = 7.2 Hz, ^4J = 1.2 Hz), 6.24 (dd, 2H, ^3J = 7.6 Hz, ^4J = 1.2 Hz), 1.57 (s, 6H). ^{13}C NMR (50 MHz, 4:1 CD_2Cl_2/CCl_4): δ 184.1, 169.2, 148.8, 148.3, 145.6, 143.4, 138.5, 137.9, 135.1, 133.9, 129.7, 124.7, 122.4, 121.5, 119.3, 115.4, 92.6, 30.5. IR (ATR, cm^{-1}): ν 3055 (w), 2997 (w), 1606 (m), 1578 (s), 1570 (s), 1476 (s), 1413 (m), 1343 (m), 1295 (m), 1331 (m), 1275 (m), 1198 (s), Scheme 1[a]

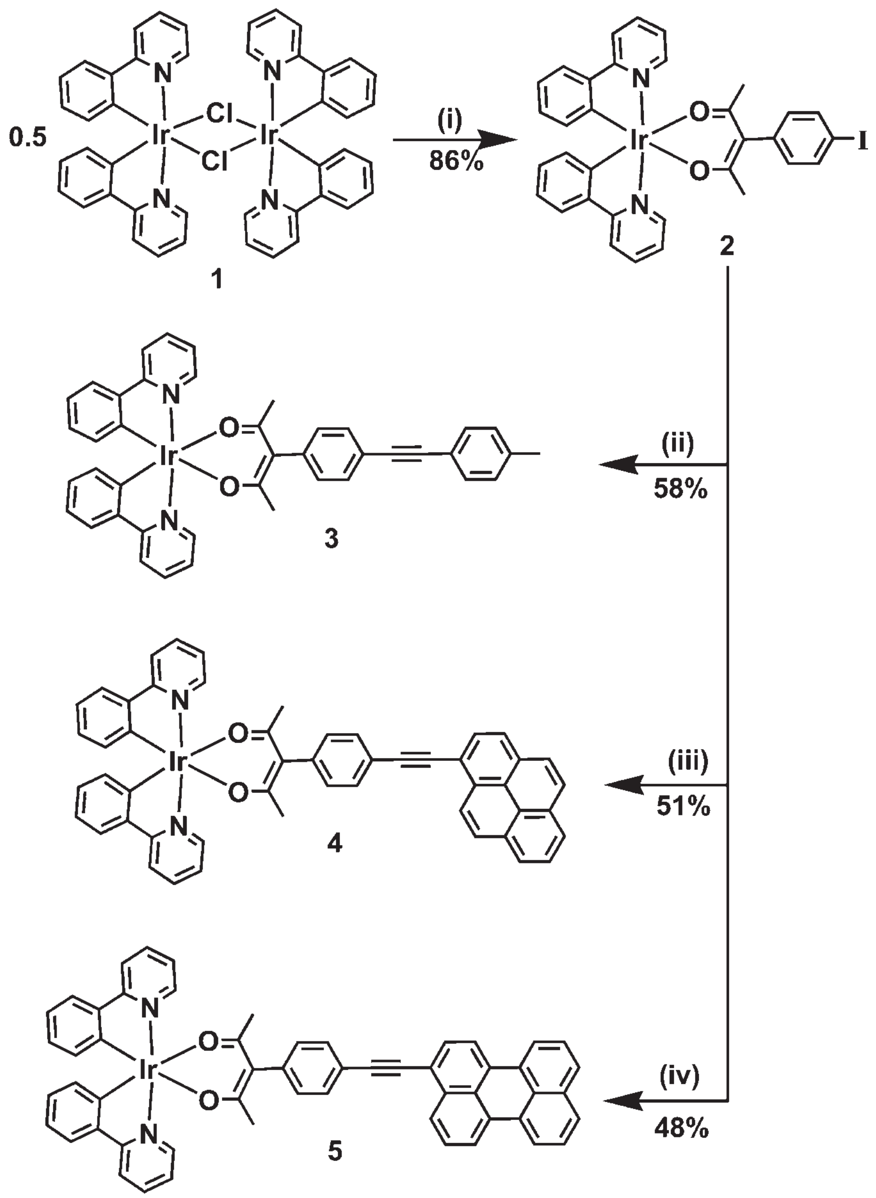

[a] (i) 4-(Acetylacetone)iodophenyl (1 equiv), *t*-BuOK (1.05 equiv), and dichloromethane, 2 h, 0 °C; then $[(ppy)_2IrCl]_2$ (0.5 equiv), 86%; (ii) 4-ethynyltoluene, benzene, triethylamine, $[Pd(PPh_3)_2Cl_2]$ (6 mol %), and CuI (10 mol %), RT, overnight, 58%; (iii) 4-ethynylpyrene, benzene, triethylamine, $[Pd(PPh_3)_2Cl_2]$ (6 mol %), and CuI (10 mol %), RT, overnight, 51%; (iv) 3-ethynylperylene, benzene, triethylamine, $[Pd(PPh_3)_2Cl_2]$ (6 mol %), and CuI (10 mol %), RT, overnight, 58%.

1060 (m), 1030 (s), 788 (s), 726 (s). UV−vis [THF; λ nm (ε, M^{-1} cm^{-1})]: 240 (17 800), 265 (21 250), 343 (4450), 414 (1780). EI-MS (nature of the peak): *m*/*z* 802.0 ([M], 100), 676.1 ([M − I + H], 35). Anal. Calcd for $C_{33}H_{26}IIrN_2O_2$: C, 49.44; H, 3.27; N, 3.49. Found: C, 49.28; H, 3.04; N, 3.19.

*Complex [(ppy)$_2$Ir(acacPhTol)] (**3**).* The general procedure was followed using **2** (87 mg, 0.109 mmol), 4-ethynyltoluene (38 mg, 41 μL, 0.327 mmol), $[Pd(PPh_3)_2Cl_2]$ (4.5 mg, 6.54 × 10^{-3} mmol), and CuI (2.0 mg, 10.9 × 10^{-3} mmol). Purification by chromatography on aluminum oxide (60:40 dichloromethane/petroleum ether) followed by crystallization by the slow diffusion of Et_2O in a CH_2Cl_2 solution gave **3** as a yellow solid (50 mg, 0.063 mmol, 58%). ^{1}H NMR (200 MHz, CD_2Cl_2): δ 8.64 (d, 2H, ^3J = 5.5 Hz), 7.95−7.79 (m, 4H), 7.60 (d, 2H, ^3J = 7.9 Hz), 7.50 (d, 2H, ^3J = 7.9 Hz), 7.42 (d, 2H, ^3J = 7.9 Hz), 7.28 (dt, 2H, ^3J = 7.2 Hz, ^4J = 1.2 Hz), 7.20−7.13 (m, 4H), 6.86 (dt, 2H, ^3J = 7.3 Hz, ^4J = 1.2 Hz), 6.69 (dt, 2H, ^3J = 7.3 Hz, ^4J = 1.2 Hz), 6.25 (d, 2H, ^3J = 6.7 Hz), 2.37 (s, 3H), 1.56 (s, 6H). ^{13}C NMR (50 MHz, C_6D_6): δ 183.9, 168.6, 148.6, 148.1, 145.4, 143.6, 139.0, 137.7, 133.6, 132.8, 132.1, 131.7, 129.5, 129.2, 124.3, 122.2, 121.8, 121.14, 120.55, 119.0, 115.68, 89.8, 89.03, 29.50, 21.60. IR (ATR, cm^{-1}): ν 3491 (w), 3039 (w), 1605 (m), 1568 (s), 1515 (w), 1475 (m), 1437 (m), 1373 (s), 1347 (m), 1295 (m), 1265 (m), 1215 (m), 1157 (m), 1060 (m), 1030 (m), 1006 (s), 831 (m), 752 (s), 728 (s). UV−vis [THF; λ nm (ε, M^{-1} cm^{-1})]: 274 (36 500), 308 (26 750), 345 (7300), 412 (2372). EI-MS (nature of the peak): *m*/*z* 790.3 ([M], 100). Anal. Calcd for $C_{42}H_{33}IrN_2O_2$: C, 63.86; H, 4.21; N, 3.55. Found: C, 64.24; H, 4.45; N, 3.79.

*Complex [(ppy)$_2$Ir(acacPhPyr)] (**4**).* The general procedure was followed using **2** (80 mg, 0.099 mmol), 1-ethynylpyrene (27 mg, 0.118 mmol), $[Pd(PPh_3)_2Cl_2]$ (4 mg, 5.69 × 10^{-3} mmol), and CuI (1.8 mg,

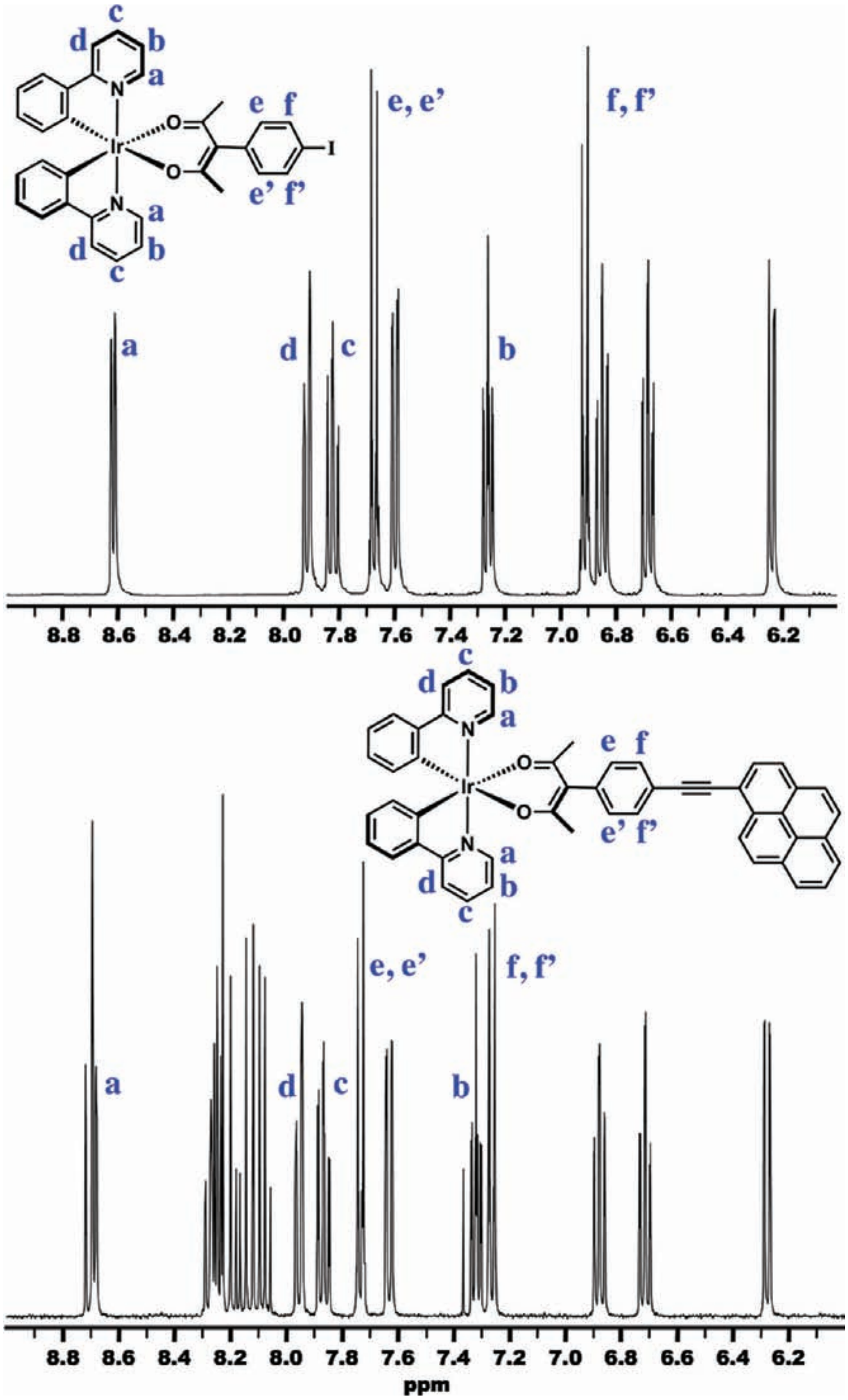

Figure 1. ^{1}H NMR spectra of **2** (top) and **4** (bottom) recorded in CD_2Cl_2. Only the aromatic region is presented.

9.9×10^{-3} mmol) Purification by chromatography on aluminum oxide (50:50 CH_2Cl_2/petroleum ether) followed by crystallization by the slow diffusion of Et_2O in a CH_2Cl_2 solution gave **4** as a yellow solid (45 mg, 0.050 mmol, 50%). ^{1}H NMR (200 MHz, CD_2Cl_2): δ 8.71−8.67 (m, 3H), 8.28−8.10 (m, 8H), 8.06−7.80 (m, 4H), 7.72 (d, 2H, ^3J = 8.0 Hz), 7.62 (d, 2H, ^3J = 7.8 Hz), 7.34−7.23 (m, 4H), 6.87 (dt, 2H, ^3J = 7.1 Hz, ^4J = 1.2 Hz), 6.70 (dt, 2H, ^3J = 7.2 Hz, ^4J = 1.2 Hz), 6.26 (d, 2H, ^3J = 7.3 Hz), 1.61 (s, 6H). ^{13}C NMR (50 MHz, CD_2Cl_2): δ 183.9, 168.7, 148.6, 148.1, 145.5, 144.0, 137.7, 133.5, 133.0, 132.3, 132.2, 131.7, 131.5, 130.0, 129.2, 128.8, 128.6, 127.6, 126.8, 126.1, 125.8, 125.0, 124.8, 124.6, 124.3, 122.3, 121.8, 121.2, 119.0, 118.2, 115.7, 95.7, 88.8, 29.5. IR (ATR, cm^{-1}): ν 3035 (w), 1605 (m), 1572 (m), 1477 (m), 1415 (m), 1375 (s), 1340 (m), 1297 (w), 1158 (w), 1060 (m), 1029 (w), 1006 (m), 970 (w), 843 (s), 822 (m), 794 (w), 754 (s), 734 (w), 714 (w). UV−vis [THF; λ nm (ε, M^{-1} cm^{-1})]: 235 (35 150), 246 (34 550), 282 (32 200), 295 (32 800), 346 (18 300), 364 (27 850), 385 (26 971), 450 (1400). EI-MS (nature of the peak): m/z 900.2 ([M], 100). Anal. Calcd for $C_{51}H_{35}IrN_2O_2$: C, 68.06; H, 3.92; N, 3.11. Found: C, 67.70; H, 3.72; N, 2.79.

*Complex [(ppy)$_2$Ir(acacPhPery)] (**5**).* The general procedure was followed using **2** (70 mg, 0.087 mmol), 3-ethynylperylene (60 mg, 0.204 mmol), [Pd(PPh_3)$_2$$Cl_2$] (3 mg, 4.27×10^{-3} mmol), and CuI (1.8 mg, 9.9×10^{-3} mmol). Purification by chromatography on aluminum oxide

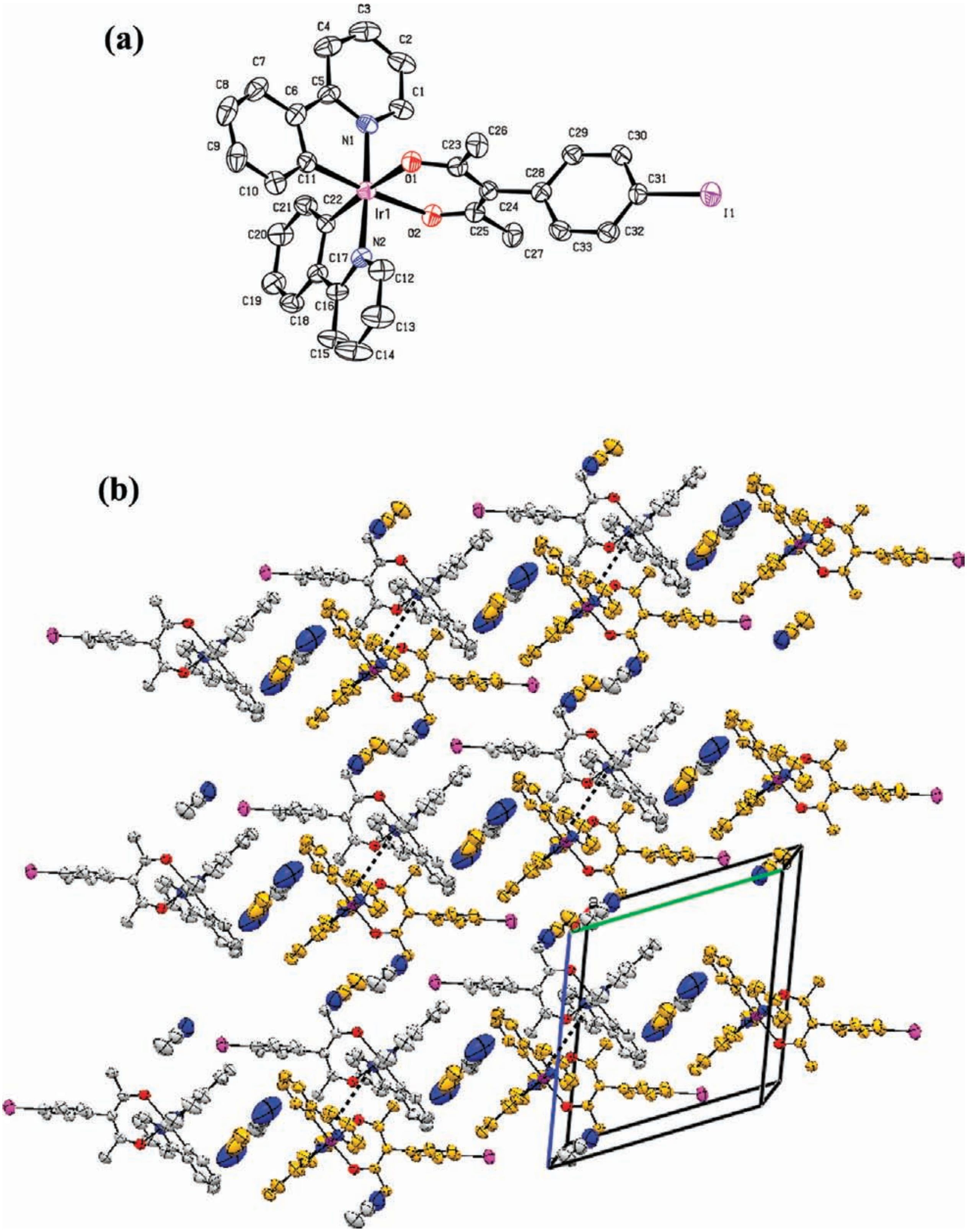

Figure 2. (a) ORTEP view of **2**. Displacement ellipsoids are drawn at the 30% probability level. (b) Projection of the crystalline structure of **2** along the *a* axis. Silver and golden colors are for inversion-related molecules. Black dashed lines indicate $\pi-\pi$-stacking interactions. Hydrogen atoms as well as the acetonitrile solvent molecules trapped during the crystallization step have been omitted for clarity.

(60:40 CH_2Cl_2/petroleum ether) followed by crystallization by the slow diffusion of Et_2O in a CH_2Cl_2 solution give **5** as a red solid (37 mg, 0.041 mmol, 48%). ^1H NMR (400 MHz, CD_2Cl_2): δ 8.66 (dd, 2H, $^3J = 6$ Hz, $^4J = 1$ Hz), 8.34−8.19 (m, 5H), 7.94 (d, 2H, $^3J = 8$ Hz), 7.85

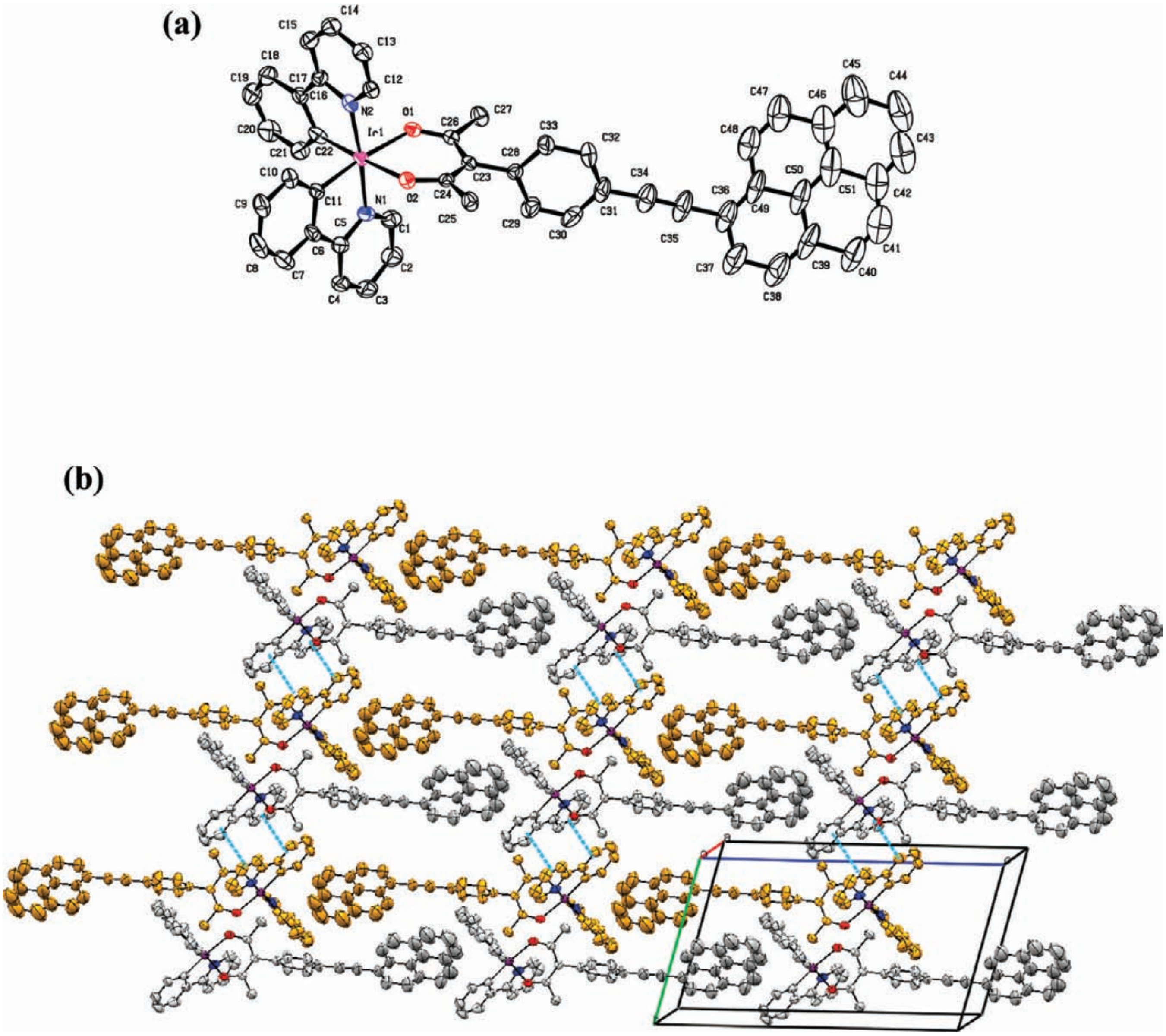

Figure 3. (a) ORTEP view of **4**. Displacement ellipsoids are drawn at the 30% probability level. (b) Projection of the crystalline structure of complex **4** along the *a* axis. Silver and golden colors are for inversion-related molecules. Light-blue dashed lines represent $\pi-\pi$-stacking interactions. (Hydrogen atoms as well as the acetonitrile solvent molecules trapped during the crystallization step have been omitted for clarity.)

(dt, 2H, ^3J = 7.6 Hz, ^4J = 1.2 Hz), 7.73 (t, 1H, ^3J = 8 Hz), 7.66−7.60 (m, 4H), 7.55−7.51 (m, 3H), 7.50 (AB quartet, 4H, ^{AB}J = 8.2 Hz, $\nu\delta_{AB}$ = 221.3 Hz), 7.30 (dt, 2H, ^3J = 6 Hz, ^1J = 1.6 Hz), 6.86 (dt, 2H, ^3J = 7.2 Hz, ^1J = 1.2 Hz), 6.70 (dt, 2H, ^3J = 7.2 Hz, ^4J = 1.6 Hz), 6.26 (dd, 2H, ^3J = 7.6 Hz, ^4J = 1 Hz), 1.60 (s, 6H). ^{13}C NMR (50 MHz, CD_2Cl_2): δ 183.6, 168.4, 149.1, 148.4, 145.2, 144.5, 138.7, 133.2, 132.8, 132.7, 132.2, 132.1, 131.7, 131.5, 130.0, 129.4, 129.1, 128.7, 128.6, 128.2, 126.3, 126.1, 125.8, 125.0, 124.8, 124.6, 124.3, 122.3, 121.8, 121.6, 118.4, 118.2, 115.7, 94.9, 88.2, 29.7. IR (ATR, cm^{-1}): ν 2920 (s), 2851 (s), 1689 (m), 1611 (m), 1566 (m), 1538 (s), 1485 (m), 1465 (m), 1429 (m), 1417 (m), 1366 (m), 1331 (m), 1275 (m), 1198 (s), 1161 (m), 1111 (s), 989 (s), 951 (m), 815 (m), 764 (m), 751 (m), 731 (m), 704 (m). UV−vis (THF; λ nm (ε, M^{-1} cm^{-1})]: 260 (35 150), 303 (12 400), 331 (9370), 414 (8400), 440 (15 000), 467 (17 709). EI-MS (nature of the peak): *m/z* 950.2 ([M], 100). Anal. Calcd for $C_{55}H_{37}IrN_2O_2$: C, 69.53; H, 3.93; N, 2.95. Found: C, 69.44; H, 3.70; N, 2.70.

■ RESULTS AND DISCUSSION

Synthesis and Characterization. The preparation of target complexes is sketched in Scheme 1. Deprotonation of the ligand (acacHPhI) is ensured using *t*-BuOK at low temperature under anhydrous conditions, and its reaction with 0.5 equiv of the iridium dimer **1** provides complex **2** after chromatographic purification over alumina.

Complexes **3**−**5** bearing distinct aromatic fragments were prepared using Sonogashira cross-coupling reactions between the appropriate acetylenic-terminated precursor and phenyliodide projecting from the acac ligand available on the preformed iridium(III) complex **2** in the presence of triethylamine. The resulting complexes were purified by flash chromatography using alumina. To illustrate the NMR structural assignments in the aromatic region, representative ^{1}H NMR spectra of complexes

Table 1. Electrochemical Data for the Heteroleptic Iridium(III) Complexes[a]

complex	$E'^{\circ}_{\mathrm{oxy}}$, V ($\Delta E$, mV)	$E'^{\circ}_{\mathrm{red}}$, V ($\Delta E$, mV)
2	+ 0.74 (60)[b]	
3	+ 0.74 (60)[b]	
1-ethnylpyrene	+1.30 (irr.)	−2.02
4	+ 0.74 (60)[b]	−1.93 (irr.)[c]
	+ 1.22 (irr.)[c]	
3-ethnylperylene	+ 1.22 (irr.)	−1.93 (irr.)
5	+ 0.74 (60)[b]	−1.72 (irr.)[d]
	+ 0.95 (60)[d]	

[a] Potentials determined by cyclic voltammetry in deoxygenated CH_2Cl_2 solutions, containing 0.1 M $TBAPF_6$, at a solute concentration of 1.5×10^{-3} M, at RT. Potentials were standardized using ferrocene (Fc) as an internal reference and converted to SCE by the relation $E_{1/2}(\mathrm{Fc/Fc^+}) = +0.38$ V ($\Delta E_p = 60$ mV) vs SCE.[52] Uncertainty in the half-wave potentials is ±10 mV. When the redox process is irreversible (irr.), the peak potentials (E_{pa} or E_{pc}) are quoted. [b] Redox process associated with the iridium center. [c] Redox process associated with pyrene. [d] Redox process associated with perylene.

2 and **4** as recorded in CD_2Cl_2 are presented in Figure 1. For the iodo derivative **2**, characteristic signals of the orthometalated ppy ligand are observed between 8.62 and 6.25 ppm. The most deshielded doublet (a) at 8.62 ppm is assigned to the two protons adjacent to the nitrogen atoms, whereas the characteristic AB quartet at 7.68 and 6.93 ppm (labeled e,e′ and f,f′) is due to the acac moiety. The well-defined spectrum is consistent with a single isomer, namely, *trans*-N,N, as confirmed by the single-crystal X-ray structure. The chemical shifts of the orthometalated ligand-based protons in **4** remain unaffected by cross-linking of the pyrene module, but the major modification is the deshielding of the AB quartet corresponding to the ancillary acac ligand (Figure 1, bottom). Similar NMR observations were revealed in **5** (Figure S1 in the Supporting Information).

X-ray Structures. Pale-yellow crystals of **2** suitable for single X-ray diffraction were grown by the slow diffusion of acetonitrile into a concentrated solution of dichloromethane. For **4**, diethyl ether replaces acetonitrile, and smaller yellow crystals were obtained. The ORTEP diagrams of **2** and **4** are depicted in Figures 2 and 3, respectively. Both complexes crystallize in the centered triclinic space group $P\bar{1}$, with one complex of interest and two solvent molecules in the asymmetric unit. Only two acetonitrile solvent molecules could be properly modeled in the X-ray structure of **2**, with the diethyl ether molecules present in the crystal of **4** being disordered. The iridium centers in complexes **2** and **4** adopt a distorted octahedral coordination geometry involving two ppy ligands and one acacPhI ligand. The ppy ligands adopt a mutual eclipsed configuration, with the N1 and N2 atoms residing in trans positions, whereas the cyclometalated carbon atoms C11 and C22 are in cis positions. All bond lengths and angles of **2** and **3** are within the normal ranges. The Ir−N distances are 2.030(4) and 2.033(4) Å for **2** [2.03(5) and 2.045(6) Å for **4**, respectively], which are longer than the Ir−C distances of 1.989(6) and 1.993(5) Å for **2** [1.969(8) and 1.993(7) Å for **4**, respectively], as seen normally in related compounds. The (acacPhI) ligand displays an O,O′-chelating coordination mode, and the distances of Ir−O are identical, with nominal values of 2.139(4) Å in **2** and slightly longer in **4** with an average distance of 2.148(5) Å. Similarly, the benzene ring directly attached to the chelating acac motif (for **2**) lies orthogonal to it, as indicated by the dihedral angle C23−C24−C28−C29 of −86.5(6)° for **2** [88.3(9)° for **4**]. Furthermore, for **4**, the mean plane of the pyrene unit is slightly twisted with respect to the phenyl ring by a dihedral angle of 17.8(4)°.

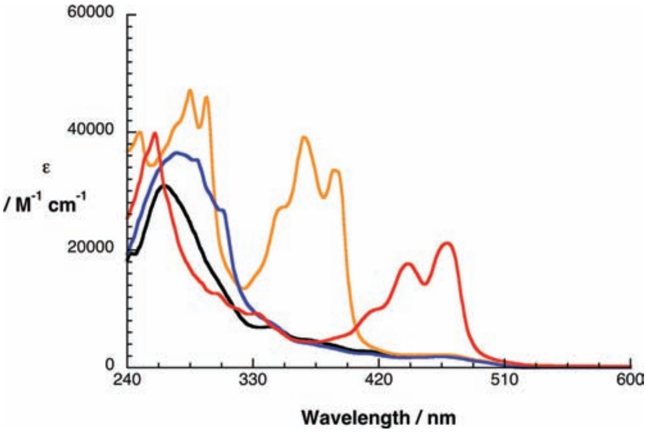

Figure 4. Electronic absorption spectra of **2** (black line), **3** (blue line), **4** (orange line), and **5** (red line) recorded in THF (2×10^{-5} M) at RT.

Electrochemistry. The electrochemical activity of complexes **2**−**5** was determined in dichloromethane using tetrabutylammonium hexafluorophosphate as the supporting electrolyte (electrochemical window from +1.7 to −2.1 V), and the results are collected in Table 1, presented as V vs SCE. All four complexes exhibit a reversible ($i_{pa}/i_{pc} \approx 1$), one-electron ($\Delta E_p = 60$ mV), metal-based oxidation at +0.74 V, demonstrating that variation in the acac ligand structure imparts no significant electronic effect on the redox activity of the iridium center.[45−47] In iridium(III) complexes, pure metal-centered oxidations are typically reversible, whereas this wave becomes quasi-reversible or irreversible when the highest occupied molecular orbital takes on more cyclometalated ligand-based character.[48,49] Without question, the one-electron reversible oxidation observed in complexes **2**−**5** must be due to the oxidation of iridium(III) to iridium(IV).[50] No cathodic redox activity could be observed for complexes **2** and **3** until the edge of the solvent window, −2.1 V. These observations are consistent with previous results obtained with $Ir(ppy)_2(acac)$.[35] The cyclic voltammogram of complex **4** shows two additional processes with respect to complex **3** due to the redox activity of the appended pyrene residue, which irreversibly oxidizes and reduces at +1.22 and −1.93 V, respectively. Under the same experimental conditions, free 1-ethynylpyrene exhibits irreversible redox activity at +1.30 and −2.02 V. These results are also in line with previous values obtained in pyrene-linked oligopyridine complexes of ruthenium(II), osmium(II), and platinum(II).[43] Please note that, in the present complexes, the redox activity of the phenylethynyl bridge falls outside our electrochemical solvent window, as has been shown in related iridium dipyrromethene,[30] or platinum ethynylene[51] complexes. This result supports the fact that this fragment is not lying in the same plane as the acac moiety because of the presence of methyl groups, which force the phenyl ring to be tilted, as is found in the presented crystal structures (vide supra). The perylene-based complex **5** also exhibits a reversible oxidation of the metal at +0.74 V and two additional redox processes assigned to that of perylene. The irreversible reduction at −1.72 V is consistent with the reduction of linked 3-ethynylperylene which is shifted

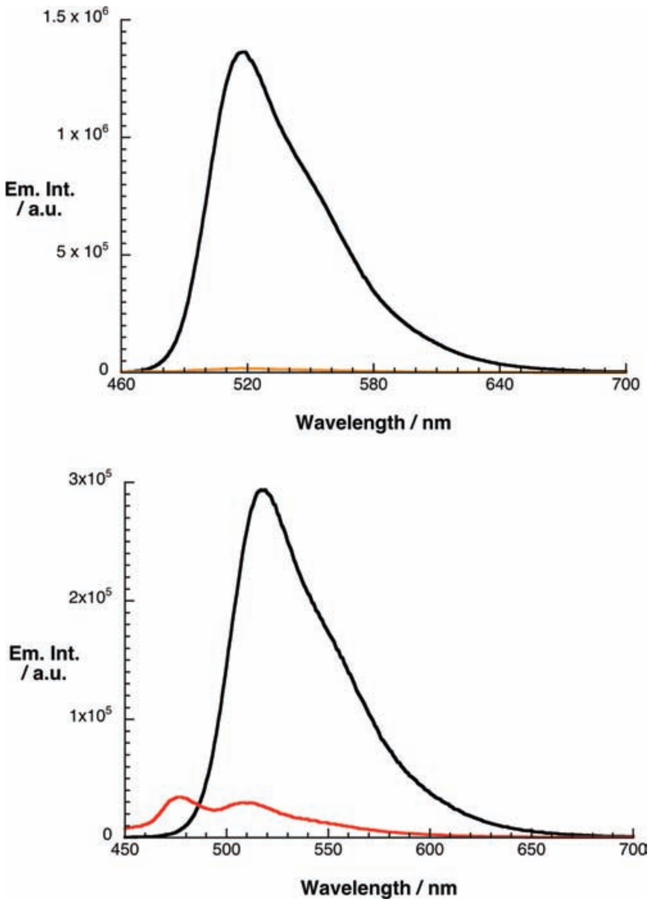

Figure 5. Top: Steady-state photoluminescence spectra of **2** (black line) and **4** (orange line), measured in deaerated THF, excited at 430 nm optically matched at the excitation wavelength. Bottom: Steady-state photoluminescence spectra of **2** (black line) and **5** (red line), measured in deaerated THF, excited at 316 nm optically matched at the excitation wavelength.

anodically by 210 mV with respect to genuine 3-ethynylperylene. On the oxidative side, the monoelectronic oxidation process of the perylene unit is observable at +0.93 V, shifted by about 270 mV in comparison to unlinked 3-ethynylperylene, which exhibits an irreversible oxidation at +1.22 V.

Electronic Spectroscopy. The electronic absorption spectrum of **2**, shown in Figure 4, exhibits characteristic absorptions from the spin-allowed intraligand $^1\pi-\pi^*$ transitions in the ultraviolet (UV) region below 300 nm. These are followed by spin-allowed metal-to-ligand charge-transfer (^{1}MLCT) transitions centered at 343 nm with an extinction coefficient of 7500 M^{-1} cm^{-1} and finally a tail into the blue region as a result of iridium-induced spin–orbit coupling promoting spin-forbidden singlet–triplet charge-transfer transitions.[53] The absorption spectra of **3**–**5** are, in general, composed of absorptions of the corresponding molecular building blocks. In **3**, the absorptions originating from the phenylacetylene subunit overlap with those of the ppy ligands, resulting in larger extinction coefficients and the appearance of two new shoulders at 290 and 308 nm. The absorption of the pyrene moiety in **4** is clearly discernible with associated maxima of 248, 285, 295, 365, and 390 nm and extinction coefficients exceeding 30 000 M^{-1} cm^{-1}. The strong red shift of the pyrene transitions, in comparison to free pyrene, is due to the core enlargement through the phenylacetylene unit and is in very good agreement with previous reports on similar structures.[9,54] The perylene-containing hybrid **5**, exhibits an additional absorption emerging from the perylene $\pi-\pi^*$ transition in the range between 400 and 510 nm with extinction coefficients of up to 20 000 M^{-1} cm^{-1}, again red-shifted with respect to free perylene due to a similar core extension, and is also in good agreement with other core-extended perylenes.[12,54]

Photoluminescence Properties. The static and dynamic photoluminescence properties of **2**–**5** were evaluated. For **2**, a characteristic RT emission from the ^{3}MLCT state was detected (Figure 5) between 470 and 660 nm with a maximum at 516 nm and a shoulder near 560 nm, measured in THF. The identical photoluminescence occurs regardless of the excitation wavelength utilized and possesses a corresponding lifetime of 1 μs in deaerated THF. The emission spectrum of **3** exhibits the same shape as **2** during excitation into any of the preceding absorption features and also exhibits an excited-state lifetime of 1 μs. In the corresponding excitation spectrum, the phenylacetylene-based transition is discernible in the UV region (Figure S2 in the Supporting Information). For **4**, the ^{3}MLCT emission is quenched by factors of 75 and 250 in THF (Figure 5, top) and acetonitrile (Figure S3 in the Supporting Information), respectively, during excitation into the optically matched low-energy absorption features. In this instance, the charge-transfer-based photoluminescence is significantly quenched, now exhibiting a lifetime of 2.1 ns at RT in acetonitrile. When this ensemble is excited with higher energy, i.e., 280 nm, a minimal amount of singlet fluorescence emanating from the pyrene moiety is discernible with maxima at 390 and 410 nm (Figure S4 in the Supporting Information). In **5**, the ^{1}MLCT transitions strongly overlap those of the $^1\pi-\pi^*$ transitions of the perylene at low energies, precluding the possibility of selective excitation of either chromophore. The photoluminescence from the ^{3}MLCT state in **5** is quantitatively quenched, and the only remaining emission features are characteristic of the perylene moiety, with maxima at 475 and 510 nm (Figure 5, bottom) and a lifetime of 2.6 ns in acetonitrile, reduced by approximately 40% in comparison to a core-extended perylene in a purely organic composition.[54]

Femtosecond Transient Absorption. For more detailed information on the processes taking place upon photoexcitation, transient absorption measurements have been carried out in oxygen-free solutions employing compound concentrations of 2×10^{-5} M at 293 K. An excitation wavelength of 420 nm was employed to exclusively excite the charge-transfer-centered transitions in **2**–**4** and the perylene subunit of **5**. To predominantly photoexcite into the pyrenyl moiety in **4** or the charge-transfer transitions of **5**, a pump wavelength of 360 nm was employed.

Upon photoexcitation of **2** into the ^{1}MLCT state, a broad transient absorption between 400 and 600 nm with a distinct maximum at 495 nm (see Figure 6, top) is discernible immediately after the impulse response function in acetonitrile. Immediately following the laser pulse, ultrafast intersystem crossing, as a result of the strong spin–orbit coupling provided by the iridium center, takes place within ~350 fs to produce the hot ^{3}MLCT state, followed by vibrational relaxation to the lowest ^{3}MLCT state. After a few picoseconds, the transient absorption features remain invariant over the whole range of our 1 ns delay line; see the bottom of Figure 6. Similar data were recorded using THF as the solvent. For **3**, transient features identical with those observed in **2** were measured.

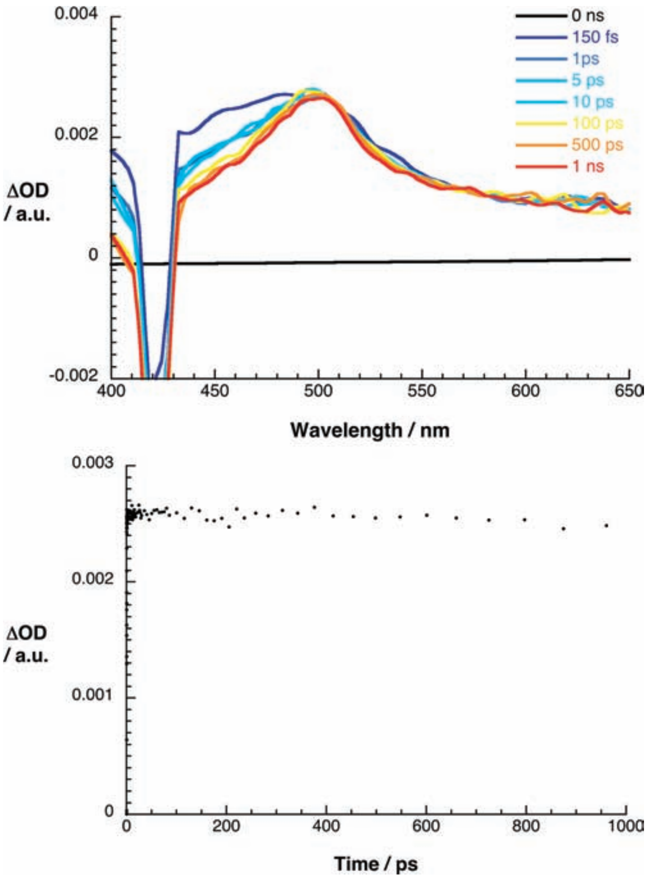

Figure 6. Top: Ultrafast transient absorption difference spectra of **2** after several time delays measured in deaerated acetonitrile excited at 420 nm. Bottom: Corresponding kinetic absorption transient recorded at 500 nm.

The transient absorption spectra of the hybrid system **4** under pulsed laser excitation at 420 nm, intended to selectively produce the ^{3}MLCT state, are presented in Figure 7, top. Instantaneously, two species are discernible: the ^{3}MLCT excited state with its maximum at 495 nm, as discussed above for **2**, and the ^{1*}pyrene state with its maximum at 480 nm. The spectral changes taking place over the next 10 ps can be assigned to an intramolecular energy redistribution from the higher vibrational levels of the ^{1*}pyrene state to the ^{3}MLCT excited state, likely accelerated through the internal heavy-metal effect of the iridium center. Afterward, the ^{3*}pyrene state is populated through intersystem crossing (^{1*}pyrene → ^{3*}pyrene) and triplet−triplet energy transfer, which can be followed within the next nanoseconds via the formation of new and more intense transients between 400 and 650 nm with maxima at 470 nm (a shoulder at 500 nm), 530, and 600 nm (see Figure 7, top). These transients were assigned, based on direct spectral comparisons, to the pyrene-centered triplet excited state, as previously published.[55] Employing an excitation wavelength of higher energy, to predominantly excite the ^{1}pyrene-based $\pi-\pi^*$ transitions, changes the initial transient spectra observed (Figure 7, center). Under this excitation condition, instantaneously the *S2 state of pyrene is discernible near 500 nm with corresponding features that extend beyond 600 nm.[56] The pyrene *S2 state deactivates over the next 0.6 and 1.9 ps (in THF and acetonitrile, respectively) to the ^{*1}pyrene excited state through vibrational cooling. Afterward, energy redistribution to the ^{3}MLCT excited state occurs in a manner similar to that presented above for **2**. We note that direct energy transfer from the pyrene *S2 state to the ^{3}MLCT excited state also represents a viable concurrent deactivation pathway for the *S2 state that cannot be ruled out. After formation of the ^{3}MLCT excited state, triplet−triplet energy transfer occurs, ultimately producing the long-lived ^{3*}pyrene state.

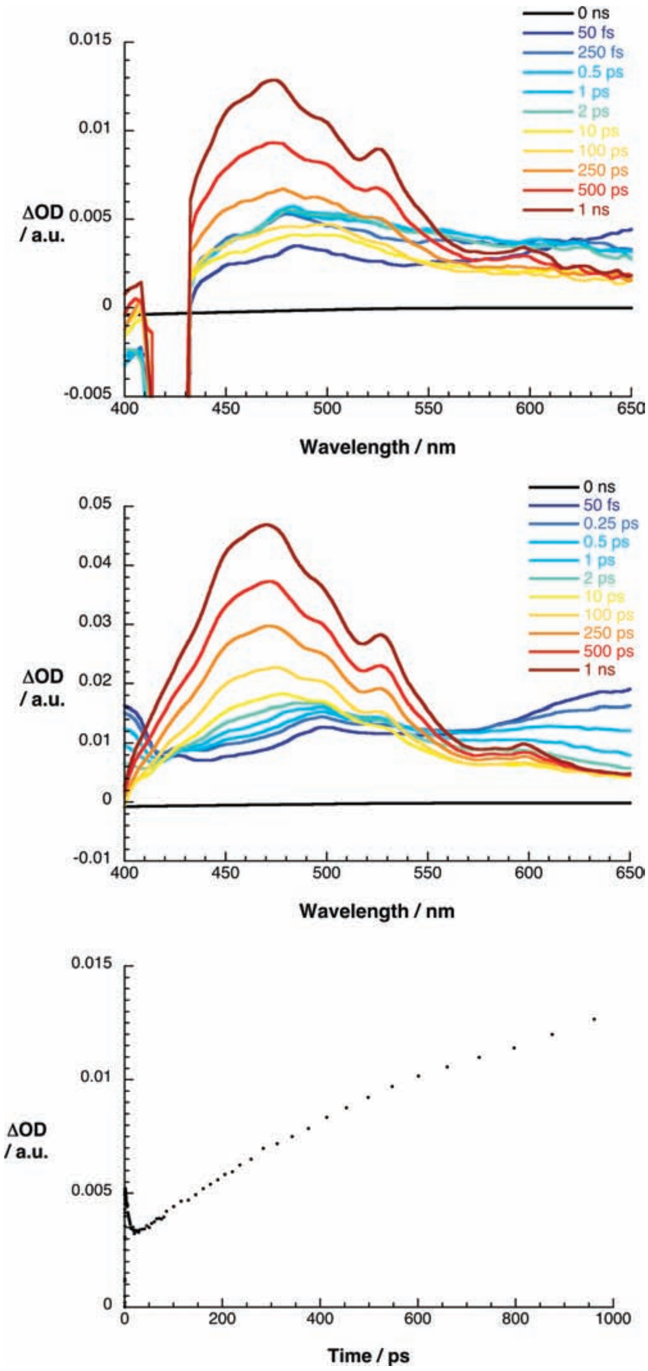

Figure 7. Top: Ultrafast transient absorption difference spectra of **4** after several time delays in deaerated acetonitrile excited at 420 nm. Center: Ultrafast transient absorption difference spectra of **4** after several time delays in deaerated acetonitrile excited at 360 nm. Bottom: Corresponding time absorption profile monitored at 470 nm following 420 nm excitation, data from top.

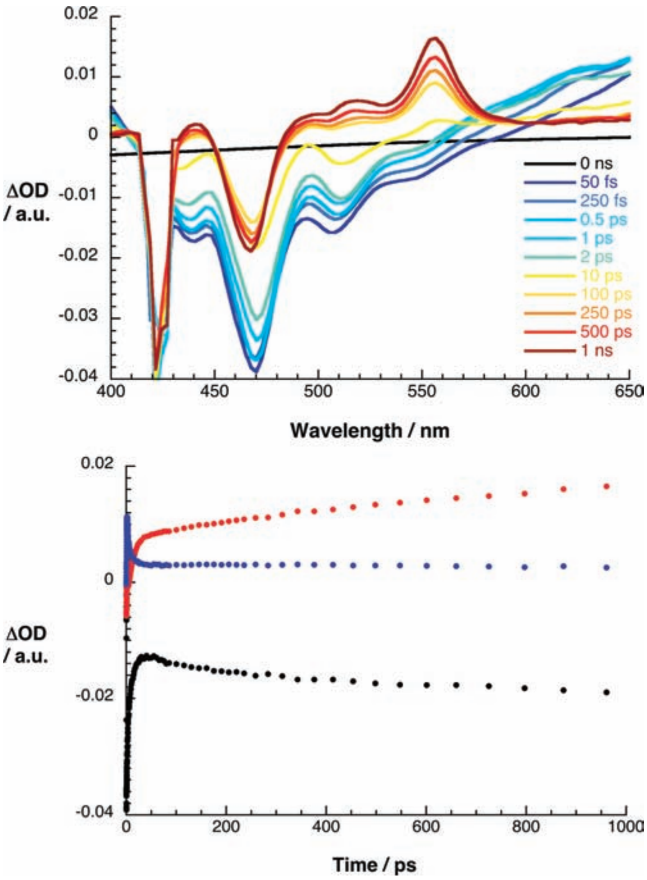

Figure 8. Top: Ultrafast transient absorption difference spectra of **5** after several time delays in deaerated acetonitrile excited at 420 nm. Bottom: Corresponding time absorption profile observed at 470 nm (black), 555 nm (red), and 625 nm (blue) of the difference spectra shown.

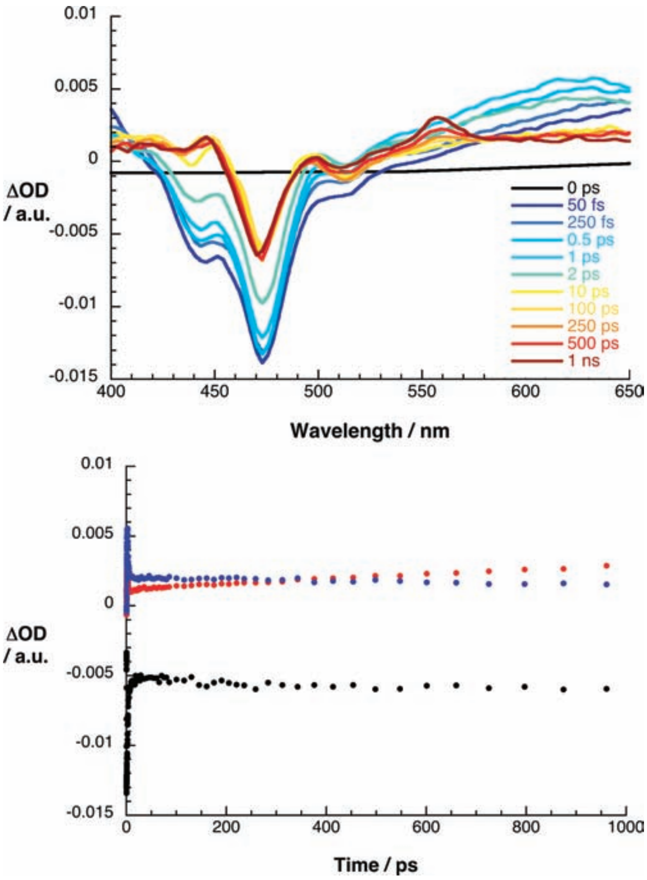

Figure 9. Top: Ultrafast transient absorption difference spectra of **5** after several time delays in deaerated acetonitrile excited at 360 nm. Bottom: Corresponding time absorption profile observed at 470 nm (black), 555 nm (red), and 625 nm (blue) of the spectra shown.

The initial difference spectrum of the perylene-containing hybrid system, when exciting with 420 nm laser pulses, is dominated by distinct ^{1*}perylene features located at 438, 473, 510, and 550 nm, followed by a maximum at 620 nm (Figure 8, top). These features convert rapidly via intersystem crossing to the corresponding ^{3*}perylene excited state, which is defined by a strong bleach at 470 nm surrounded by maxima at both higher and lower energies at 440, 520, and 560 nm. After 10 ps, these latter features dominate the whole visible region, and after 50 ps, all transients associated with the ^{1*}perylene state features are no longer observed. The longer-lifetime component, as reflected through the corresponding time absorption profile (Figure 8, bottom), is believed to be due to triplet−triplet energy transfer from the ^{3}MLCT state, whose features are hidden beneath the much more intense perylene features.

Excitation into the transition centered at 360 nm leads to the population of the *S2 state of the perylene moiety, which dominates the entire spectral window (Figure 9). From this *S2 state, a number of competitive processes occur: vibrational cooling to the ^{1*}perylene state, direct intersystem crossing to the ^{3*}perylene state, and energy migration to the ^{3}MLCT state taking place over the first 3 ps. After 10 ps, the whole visible range is dominated by the ^{3*}perylene transient features with an indication of minor formed ^{1*}perylene state features clearly observable by the ground-state bleach, i.e., at 430 nm. Within the next nanosecond, the ^{3*}perylene features increase in intensity, which can be followed at the ^{3*}perylene triplet marker at 555 nm, because of the triplet−triplet energy transfer from the ^{3}MLCT state.

Nanosecond Transient Absorption. The nansecond transient absorption difference spectra of the hybrids and the reference compounds measured at select delay times following nanosecond laser pulses are presented in Figure 10. The current data obtained on an iCCD detector provide non-emission-corrected spectral difference profiles for compounds **2**, **4**, and **5** between 400 and 800 nm.

The transient absorption difference spectrum of **2** contains the features characteristic of the ^{3}MLCT state. The difference of the spectral shape, in comparison to the femtosecond transient absorption spectra, is given by the fact that also phosphorescence is detected, reflected by the apparent strong bleach between 490 and 640 nm. The recovery of the ground state determined via observation of the triplet absorption features occurs with a time constant of 1 μs, in perfect agreement to the value determined in the emission lifetime experiment. Complex **3** displays identical transient features (data not shown) with a lifetime of 1 μs in THF and 890 ns in acetonitrile. For **4**, the ^{3*}pyrene state dominates the entire visible range and is discernible with maxima at 480, 540, and 600 nm, followed by a much weaker shoulder at 650 nm, similar to the observations in the ultrafast transient absorption experiment at 1 ns delay and in good agreement with previous reports.[9,57] The recovery of the ground state follows afterward within 40 and 20 μs respectively in THF and acetonitrile.[58]

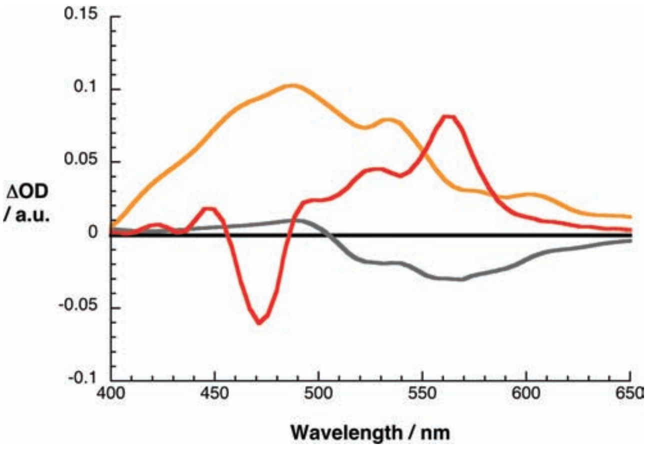

Figure 10. Nanosecond transient absorption difference spectra of **2** (gray line), **4** (orange line), and **5** (red line) recorded 100 ns after a 465 nm laser pulse, measured in deaerated THF.

Scheme 2. Energy Level Diagram Depicting the Relevant Spectroscopic States in 4 and 5

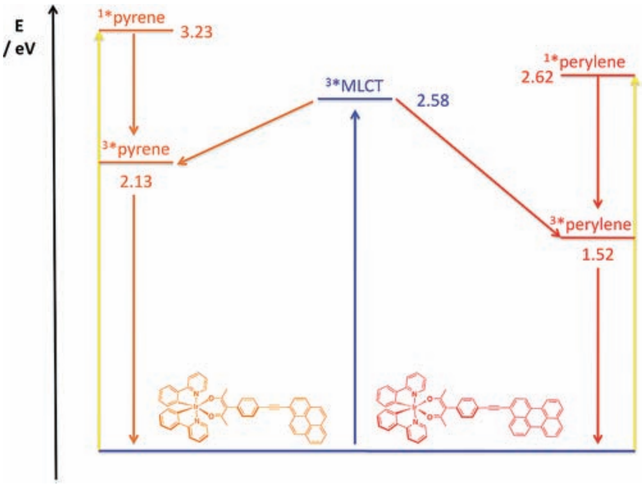

In **5**, the difference spectra observed in the nanosecond transient absorption show the well-known features of the ^{3*}perylene excited state, with three weak maxima before the intense ground-state bleach at 470 nm and three intense transition afterward at 490, 520, and 565 nm.[12] The lifetime of the triplet excited state was determined to be 82 and 30 μs in oxygen-free THF and acetonitrile solutions, respectively.

Energetics. Comparing the energetics with the molecular orbital levels helps one to comprehend the relevant mechanisms of excited-state deactivation. First, **2** and **3** instantaneously form the ^{3}MLCT state upon photoirradiation. Even during excitation into the ^{1}IL or ^{1}MLCT transitions, ultrafast relaxation accelerated by strong spin−orbit coupling favors intersystem crossing to the ^{3}MLCT state, which is located at 2.58 eV. Afterward, the recovery of the ground state occurs through both radiative (phosphorescence) and nonradiative processes in both molecules because there are no low-lying triplet states in kinetic competition.

The additional orbital levels localized on 1-ethynylpyrene in **4** enable new pathways for deactivation upon photoexcitation, as presented in Scheme 2. During pumping into the iridium charge-transfer states, still located at 2.58 eV, only one of them, triplet−triplet energy transfer to the pyrene triplet excited state located at 2.13 eV, is favorable.[57] Populating the ^{1*}pyrene state, located at 3.23 eV, results into two competing pathways, intersystem crossing to the ^{3*}pyrene state and the energy redistribution to the ^{3}MLCT state, with the latter pathway dominating excited-state decay out of higher-lying vibrational levels. Predominant photoexcitation of the *S2 state of the pyrene subunit results in even faster energy redistribution to the ^{3}MLCT state. Subsequent to triplet−triplet energy transfer, the final manifold ultimately populated in **4** that regenerates the ground state is the ^{3*}pyrene state. Similarly, the dynamics of **5** follow precisely pathways identical with those discussed above for **4**. Any population of the ^{3}MLCT state is immediately followed by triplet−triplet energy transfer to the lower-lying ^{3*}perylene state, where the excitation energy finally localizes and slowly decays to reform the molecular ground state. The ^{3}MLCT state can be populated either directly or via energy redistribution from the *S1 or *S2 state of the perylene, with respective rate constants of 1.0×10^{11} and 3.3×10^{11} s^{-1}. Such long-lived triplet excited states appear poised to serve as sensitizers for a variety of applications including solar fuel photochemistry,[59] singlet oxygen production,[6,60] and photon upconversion based on sensitized triplet−triplet annihilation.[61]

■ CONCLUSION

In summary, we have synthesized and investigated the photophysical properties of a series of new iridium(III) charge-transfer chromophores bearing a lone extended-core tolyl (**3**), pyrenyl (**4**), or perylenyl (**5**) subunit, each constructed using the "chemistry on the complex" approach. The iodo precursor synthon **2**, along with the tolyl-substituted **3**, each exhibit charge-transfer-based photoluminescence ($\tau \sim 1\ \mu$s at RT), whereas this emission is nearly quantitatively quenched, regardless of the excitation wavelength, in both **4** and **5**. Ultrafast transient absorption spectroscopy revealed that, regardless of the mode of excitation in **4** and **5**, the lowest-energy ligand-localized triplet state inevitably becomes populated in each instance and is readily identified as the extended-core ^{3*}pyrene or ^{3*}perylene in nature, respectively. Conventional laser flash photolysis was used to determine the excited-state lifetimes of these triplets, which are on the order of tens of microseconds, depending upon the nature of the solvent.

■ ASSOCIATED CONTENT

Ⓢ Supporting Information. X-ray crystallographic data in CIF format, experimental details for the photophysical characterization, additional ^{1}H NMR, and photoluminescence data. This material is available free of charge via the Internet at http://pubs.acs.org.

■ AUTHOR INFORMATION

Corresponding Authors

*E-mail: castell@bgsu.edu (F.N.C.), ziessel@unistra.fr (R.Z.). Fax: +1 419 372-9809.

■ ACKNOWLEDGMENT

This work was supported by the NSF (Grant CHE-1012487), the AFOSR (Grant FA9550-05-1-0276), the BGSU Research

Enhancement Initiative, the Center National de la Recherche Scientifique, and the University de Strasbourg. Dr. Alexander Tarnovsky is gratefully acknowledged for providing generous access to and experimental assistance with the femtosecond transient absorption pump−probe experiment.

■ REFERENCES

(1) Castellano, F. N.; Pomestchenko, I. E.; Shikhova, E.; Hua, F.; Muro, M. L.; Rajapakse, N. *Coord. Chem. Rev.* **2006**, *250* (13−14), 1819–1828.

(2) Williams, J. A. G. Photochemistry and Photophysics of Coordination Compounds: Platinum. In *Topics in Current Chemistry—Photochemistry and Photophysics of Coordination Compounds II*; Balzani, V., Campagna, S., Eds., Springer: Berlin, 2007; Vol. 281, pp 205−268.

(3) You, Y.; Park, S. Y. *Dalton Trans.* **2009**, *8*, 1267–1282.

(4) Muro, M. L.; Rachford, A. A.; Wang, X.; Castellano, F. N. Platinum(II) Acetylide Photophysics. In *Topics in Organometallic Chemistry—Photophysics of Organometallics*; Lees, A. J., Ed.; Springer-Verlag: Berlin, 2010; Vol. 29, pp 159−191.

(5) Rausch, A. F.; Homeier, H. H. H.; Yersin, H. Organometallic Pt(II) and Ir(III) Triplet Emitters for OLED Applications and the Role of Spin−Orbit Coupling: A Study Based on High-Resolution Optical Spectroscopy. In *Topics in Organometallic Chemistry—Photophysics of Organometallics*; Lees, A. J., Ed;. Springer: Berlin, 2010; Vol. 29, pp 193−235.

(6) Rachford, A. A.; Hua, F.; Adams, C. J.; Castellano, F. N. *Dalton Trans.* **2009**, *20*, 3950–3954.

(7) Adams, C. J.; Fey, N.; Weinstein, J. A. *Inorg. Chem.* **2006**, *45* (16), 6105–6107.

(8) Pomestchenko, I. E.; Luman, C. R.; Hissler, M.; Ziessel, R.; Castellano, F. N. *Inorg. Chem.* **2003**, *42* (5), 1394–1396.

(9) Danilov, E. O.; Pomestchenko, I. E.; Kinayyigit, S.; Gentili, P. L.; Hissler, M.; Ziessel, R.; Castellano, F. N. *J. Phys. Chem. A* **2005**, *109* (11), 2465–2471.

(10) Goeb, S.; Rachford, A. A.; Castellano, F. N. *Chem. Commun.* **2008**, *7*, 814–816.

(11) Rachford, A. A.; Goeb, S.; Castellano, F. N. *J. Am. Chem. Soc.* **2008**, *130* (9), 2766–2767.

(12) Rachford, A. A.; Goeb, S.; Ziessel, R.; Castellano, F. N. *Inorg. Chem.* **2008**, *47* (10), 4348–4355.

(13) Guo, H.; Muro-Small, M. L.; Ji, S.; Zhao, J.; Castellano, F. N. *Inorg. Chem.* **2010**, *49* (15), 6802–6804.

(14) Goeb, S.; Prusakova, V.; Wang, X.; Vezinat, A.; Salle, M.; Castellano, F. N. *Chem. Commun.* **2011**, *47* (15), 4397–4399.

(15) Lowry, M. S.; Bernhard, S. *Chem.—Eur. J.* **2006**, *12* (31), 7970–7977.

(16) Waern, J. B.; Desmarets, C.; Chamoreau, L.-M.; Amouri, H.; Barbieri, A.; Sabatini, C.; Ventura, B.; Barigelletti, F. *Inorg. Chem.* **2008**, *47* (8), 3340–3348.

(17) Zhao, Q.; Li, F.; Huang, C. *Chem. Soc. Rev.* **2010**, *39* (8), 3007–3030.

(18) Zhao, Q.; Huang, C.; Li, F. *Chem. Soc. Rev.* **2011**, *40* (5), 2508–2524.

(19) Lo, K. K.-W.; Li, S. P.-Y.; Zhang, K. Y. *New J. Chem.* **2011**, *35* (2), 265–287.

(20) Adachi, C.; Baldo, M. A.; Forrest, S. R.; Thompson, M. E. *Appl. Phys. Lett.* **2000**, *77* (6), 904–906.

(21) Lamansky, S.; Djurovich, P.; Murphy, D.; Abdel-Razzaq, F.; Lee, H.-E.; Adachi, C.; Burrows, P. E.; Forrest, S. R.; Thompson, M. E. *J. Am. Chem. Soc.* **2001**, *123* (18), 4304–4312.

(22) (a) Stagni, S.; Colella, S.; Palazzi, A.; Valenti, G.; Zacchini, S.; Paolucci, F.; Marcaccio, M.; Albuquerque, R. Q.; De Cola, L. *Inorg. Chem.* **2008**, *47* (22), 10509–10521. (b) Yang, C.-H.; Beltran, J.; Lemaur, V.; Cornil, J.; Hartmann, D.; Sarfert, W.; Froöhlich, R.; Bizzarri, C.; De Cola, L. *Inorg. Chem.* **2010**, *49* (21), 9891–9901.

(23) (a) Chou, P.-T.; Chi, Y. *Chem.—Eur. J.* **2007**, *13*, 380–395. (b) Chiu, Y.-C.; Hung, J.-Y.; Chi, Y.; Chen, C.-C.; Chang, C.-H.; Wu, C.-C.; Cheng, Y.-M.; Yu, Y.-C.; Lee, G.-H.; Chou, P.-T. *Adv. Mater.* **2009**, *21*, 2221–2225. (c) Duan, H.-S.; Chou, P.-T.; Hsu, C.-C.; Hung, J.-Y.; Chi, Y. *Inorg. Chem.* **2009**, *48*, 6501–6508.

(24) Adachi, C.; Baldo, M. A.; Thompson, M. E.; Forrest, S. R. *J. Appl. Phys.* **2001**, *90* (10), 5048–5051.

(25) Zhao, W.; Castellano, F. N. *J. Phys. Chem. A* **2006**, *110* (40), 11440–11445.

(26) Dixon, I. M.; Collin, J.-P.; Sauvage, J.-P.; Flamigni, L. *Inorg. Chem.* **2001**, *40* (22), 5507–5517.

(27) Goze, C.; Kozlov, D. V.; Castellano, F. N.; Suffert, J.; Ziessel, R. *Tetrahedron Lett.* **2003**, *44* (48), 8713–8716.

(28) Kozlov, D. V.; Tyson, D. S.; Goze, C.; Ziessel, R.; Castellano, F. N. *Inorg. Chem.* **2004**, *43* (19), 6083–6092.

(29) Sun, Y.-H.; Zhu, X.-H.; Chen, Z.; Zhang, Y.; Cao, Y. *J. Org. Chem.* **2006**, *71* (16), 6281–6284.

(30) Rachford, A. A.; Ziessel, R.; Bura, T.; Retailleau, P.; Castellano, F. N. *Inorg. Chem.* **2010**, *49* (8), 3730–3736.

(31) Tsuboyama, A.; Iwawaki, H.; Furugori, M.; Mukaide, T.; Kamatani, J.; Igawa, S.; Moriyama, T.; Miura, S.; Takiguchi, T.; Okada, S.; Hoshino, M.; Ueno, K. *J. Am. Chem. Soc.* **2003**, *125* (42), 12971–12979.

(32) Baldo, M. A.; Thompson, M. E.; Forrest, S. R. *Nature* **2000**, *403* (6771), 750–753.

(33) Montes, V. A.; Pérez-Bolívar, C.; Agarwal, N.; Shinar, J.; Anzenbacher, P. *J. Am. Chem. Soc.* **2006**, *128* (38), 12436–12438.

(34) Olivier, J.-H.; Haefele, A.; Retailleau, P.; Ziessel, R. *Org. Lett.* **2009**, *12* (3), 408–411.

(35) Lamansky, S.; Djurovich, P.; Murphy, D.; Abdel-Razzaq, F.; Kwong, R.; Tsyba, I.; Bortz, M.; Mui, B.; Bau, R.; Thompson, M. E. *Inorg. Chem.* **2001**, *40* (7), 1704–1711.

(36) You, Y.; Kim, K. S.; Ahn, T. K.; Kim, D.; Park, S. Y. *J. Phys. Chem. C* **2007**, *111* (10), 4052–4060.

(37) Nonius, B. V. *COLLECT—data collection software*; Springer, Delft, The Netherlands, 1999.

(38) Otwinowski, Z.; Minor, W. Methods in Enzymology. In *Macromolecular Crystallography, Part A*; Carter, C. W. J., Sweet, R. M., Eds.; Academic Press: New York, 1997; Vol. 276.

(39) Sheldrick, G. *Acta Crystallogr., Sect. A* **2008**, *64* (1), 112–122.

(40) Spek, A. *Acta Crystallogr., Sect. D* **2009**, *65* (2), 148–155.

(41) King, K. A.; Spellane, P. J.; Watts, R. J. *J. Am. Chem. Soc.* **1985**, *107* (5), 1431–1432.

(42) Dangles, O.; Guibe, F.; Balavoine, G.; Lavielle, S.; Marquet, A. *J. Org. Chem.* **1987**, *52* (22), 4984–4993.

(43) Hissler, M.; Harriman, A.; Khatyr, A.; Ziessel, R. *Chem.—Eur. J.* **1999**, *5* (11), 3366–3381.

(44) Inouye, M.; Hyodo, Y.; Nakazumi, H. *J. Org. Chem.* **1999**, *64* (8), 2704–2710.

(45) Didier, P.; Ortmans, I.; Kirsch-De Mesmaeker, A.; Watts, R. J. *Inorg. Chem.* **1993**, *32* (23), 5239–5245.

(46) Serroni, S.; Juris, A.; Campagna, S.; Venturi, M.; Denti, G.; Balzani, V. *J. Am. Chem. Soc.* **1994**, *116* (20), 9086–9091.

(47) Polson, M.; Fracasso, S.; Bertolasi, V.; Ravaglia, M.; Scandola, F. *Inorg. Chem.* **2004**, *43* (6), 1950–1956.

(48) Calogero, G.; Giuffrida, G.; Serroni, S.; Ricevuto, V.; Campagna, S. *Inorg. Chem.* **1995**, *34* (3), 541–545.

(49) Neve, F.; La Deda, M.; Crispini, A.; Bellusci, A.; Puntoriero, F.; Campagna, S. *Organometallics* **2004**, *23* (24), 5856–5863.

(50) Kim, J. I.; Shin, I.-S.; Kim, H.; Lee, J.-K. *J. Am. Chem. Soc.* **2005**, *127* (6), 1614–1615.

(51) Ventura, B.; Barbieri, A.; Zanelli, A.; Barigelletti, F.; Seneclauze, J. B.; Diring, S.; Ziessel, R. *Inorg. Chem.* **2009**, *48* (14), 6409–6416.

(52) Pavlishchuk, V. V.; Addison, A. W. *Inorg. Chim. Acta* **2000**, *298* (1), 97–102.

(53) You, Y.; Huh, H. S.; Kim, K. S.; Lee, S. W.; Kim, D.; Park, S. Y. *Chem. Commun.* **2008**, *34*, 3998–4000.

(54) Harriman, A.; Mallon, L.; Ziessel, R. *Chem.—Eur. J.* **2008**, *14* (36), 11461–11473.

(55) Samori, S.; Tojo, S.; Fujitsuka, M.; Yang, S.-W.; Ho, T.-I.; Yang, J.-S.; Majima, T. *J. Phys. Chem. B* **2006**, *110* (26), 13296–13303.

(56) Raytchev, M.; Pandurski, E.; Buchvarov, I.; Modrakowski, C.; Fiebig, T. *J. Phys. Chem. A* **2003**, *107* (23), 4592–4600.

(57) Harriman, A.; Hissler, M.; Ziessel, R. *Phys. Chem. Chem. Phys.* **1999**, *1* (18), 4203–4211.

(58) In both solvents, THF and acetonitrile, a biexponential fit had to be utilized to determine the lifetime of deactivation, with longer components of 144 and 80 μs. The lifetime of the triplet excited state was determined through bimolecular quenching of the pyrene triplet excited state with anthracene (not shown). While the fast component was quenched when the quencher concentration was increased, the slow component was unaffected.

(59) Esswein, A. J.; Nocera, D. G. *Chem. Rev.* **2007**, *107* (10), 4022–4047.

(60) Danilov, E. O.; Rachford, A. A.; Goeb, S.; Castellano, F. N. *J. Phys. Chem. A* **2009**, *113* (19), 5763–5768.

(61) Singh-Rachford, T. N.; Castellano, F. N. *Coord. Chem. Rev.* **2010**, *254* (21–22), 2560–2573.